RESEARCH ARTICLE

Multimodal imaging of murine cerebrovascular dynamics induced by transcranial pulse stimulation

Maria Eleni Karakatsani[1,2] 🄳 | Daniil Nozdriukhin[1,2] | Savannah Tiemann[1,2] |
Hikari A. I. Yoshihara[1,2] | Rafael Storz[3] | Markus Belau[3] | Ruiqing Ni[1,4] |
Daniel Razansky[1,2] | Xosé Luís Deán-Ben[1,2]

[1]Institute for Biomedical Engineering and Institute of Pharmacology and Toxicology, Faculty of Medicine, University of Zurich, Zurich, Switzerland

[2]Institute for Biomedical Engineering, Department of Information Technology and Electrical Engineering, ETH Zurich, Zurich, Switzerland

[3]Storz Medical AG, Tagerwilen, Switzerland

[4]Institute for Regenerative Medicine, Faculty of Medicine, University of Zurich, Zurich, Switzerland

Correspondence
Daniel Razansky and Xosé Luís Deán-Ben, Institute for Biomedical Engineering, University and ETH Zürich, Wolfgang-Pauli-Strasse 27, 8093 Zurich, Switzerland.
Email: daniel.razansky@uzh.ch and xl.deanben@pharma.uzh.ch

Funding information
Innosuisse – Swiss Innovation Agency, Grant/Award Number: 51767.1 IP-LS; National Institutes of Health, Grant/Award Number: RF1-NS126102

Abstract

INTRODUCTION: Transcranial pulse stimulation (TPS) is increasingly being investigated as a promising potential treatment for Alzheimer's disease (AD). Although the safety and preliminary clinical efficacy of TPS short pulses have been supported by neuropsychological scores in treated AD patients, its fundamental mechanisms are uncharted.

METHODS: Herein, we used a multi-modal preclinical imaging platform combining real-time volumetric optoacoustic tomography, contrast-enhanced magnetic resonance imaging, and ex vivo immunofluorescence to comprehensively analyze structural and hemodynamic effects induced by TPS. Cohorts of healthy and AD transgenic mice were imaged during and after TPS exposure at various per-pulse energy levels.

RESULTS: TPS enhanced the microvascular network, whereas the blood–brain barrier remained intact following the procedure. Notably, higher pulse energies were necessary to induce hemodynamic changes in AD mice, arguably due to their impacted vessels.

DISCUSSION: These findings shed light on cerebrovascular dynamics induced by TPS treatment, and hence are expected to assist improving safety and therapeutic outcomes.

Highlights:

· Transcranial pulse stimulation (TPS) facilitates transcranial wave propagation using short pulses to avoid tissue heating.

· Preclinical multi-modal imaging combines real-time volumetric optoacoustic (OA) tomography, contrast-enhanced magnetic resonance imaging (CE-MRI), and ex vivo immunofluorescence to comprehensively analyze structural and hemodynamic effects induced by TPS.

Maria Eleni Karakatsani and Daniil Nozdriukhin have contributed equally in this study.

- Blood volume enhancement in microvascular networks was reproducibly observed with real-time OA imaging during TPS stimulation.
- CE-MRI and gross pathology further confirmed that the brain architecture was maintained intact without blood–brain barrier (BBB) opening after TPS exposure, thus validating the safety of the procedure.
- Higher pulse energies were necessary to induce hemodynamic changes in AD compared to wild-type animals, arguably due to their pathological vessels.

KEYWORDS

Alzheimer's disease, blood–brain barrier, brain hemodynamics, magnetic resonance imaging, mouse models, optoacoustic imaging, therapeutic ultrasound, transcranial pulsed stimulation

1 | INTRODUCTION

As the leading cause of dementia affecting ≈50 million people worldwide, Alzheimer's disease (AD) profoundly impacts the lives of patients and their families, imposing an ever-increasing demand for social and health care resources amid a rapidly aging global population.[1–3] Therapies based on drugs, non-pharmacological activities, and mental support focus mainly on symptomatic relief and life quality improvement.[4–6] The limited effectiveness of these methods underscores the need for a deeper understanding of the basic disease mechanisms, potentially leading to viable therapeutic alternatives.

Ultrasound has long been used to act on the human brain with high spatial and/or temporal precision.[7] Recently, new effects induced by focused ultrasound (FUS) on cerebral areas have been discovered, and FUS-based methods are increasingly being investigated as promising therapies for neurological disorders, such as AD, Parkinson's disease, essential tremor, and others.[8–12] FUS is known to cause mechanical and/or thermal effects that depend on the sonication frequency, intensity, pulse or burst duration, and infusion of microbubbles, among other factors.[13,14] The mechanical effects of the cavitational forces on the blood–brain barrier (BBB) are known to loosen the tight junctions and facilitate agent delivery into the brain parenchyma. Moreover, FUS-induced BBB opening has been proven beneficial, even in the absence of a deliverable compound, suggesting the activation of modulatory mechanisms.[15]

TPS differs from other ultrasound-based brain stimulation techniques that often induce tissue heating through continuous or long-duration pulses.[16] Instead, TPS utilizes individual short pulses that produce mechanical effects without causing any increase in tissue temperature.[17,18] TPS pulses are dominated by low-frequency content, which facilitates transcranial propagation while avoiding reflected and standing waves. Preclinical evidence of TPS safety was demonstrated in rats,[17] and several clinical studies have suggested a potential modulatory impact on cortical thickness and regional atrophy.[18–20] Independent studies on treated AD patients showed significantly improved neuropsychological scores lasting up to 3 months, which were consistent with the upregulation of memory networks observed in functional magnetic resonance imaging (fMRI) data.[17,21] Extended TPS treatment over longer durations indicates that it may improve AD symptoms over several years.[22] TPS is clinically certified for AD therapy according to the European Conformity (CE) mark and is expected to play an important role in the clinical management of the disease. However, the primary mechanism and the downstream effects of TPS have not been studied, which hinders optimization of the treatment regimen and a broader clinical adoption of the technique.

In this work we conducted a systematic preclinical study focused on a thorough analysis of the immediate vascular and hemodynamic effects induced by TPS in the murine brain. Healthy and transgenic mice recapitulating AD-related phenotypes in humans were imaged during and after TPS stimulation with a state-of-the-art, real-time, cross-sectional optoacoustic (OA) tomography system and an advanced high-field MRI scanner equipped with a cryogenic surface coil. The in vivo results were validated with bright-field images of ex vivo brain sections and confocal microscopy. The primary outcome of the study aims to characterize the safety profile of the TPS application and provide valuable suggestions for clinical optimization.

2 | MATERIALS AND METHODS

2.1 | Animal experiments

The animals used in this study were housed in ventilated cages in a controlled temperature (21 ± 1°C) and humidity (55 ± 10%) environment under a 12 h dark/light cycle. Palleted food and water were provided ad libitum. All experiments were, conducted in accordance with the Swiss Federal Act on Animal Protection and approved by the Cantonal Veterinary Office Zürich.

All animals were initially anesthetized with a mixture of oxygen-air and isoflurane at 100-400 mL/min, 5% v/v for induction and 2% v/v for maintenance (Abbott, Cham, Switzerland). The animals were placed on a heated bed in a prone position with their heads fixed into a custom-designed stereotactic holder coupled with a breathing mask. To minimize acoustic impedance mismatch and ensure TPS efficiency,

RESEARCH IN CONTEXT

1. **Systematic review**: Articles relevant to transcranial pulse stimulation (TPS), optoacoustic (OA) tomography, and Alzheimer's disease (AD) were identified by electronic databases, PubMed and Google Scholar. Further relevant articles were selected from the reference lists included in the research studies we reviewed. We have focused primarily on studies applying therapeutic ultrasound in the brain, the in vivo and ex vivo imaging methods frequently used to visualize the brain vasculature and structure, and the quantitative outcomes that indicate therapeutic effects.

2. **Interpretation**: Blood volume increase in microvascular networks and intact blood–brain barrier following TPS application were observed. Higher pulse energies were necessary to induce hemodynamic changes in AD mice, attributed to their affected vessels. Our study suggests that the energy level delivered by the clinically approved TPS handpiece (Neurolith, Storz Medical AG, Switzerland) should be determined according to the patients' cerebrovascular and ventricular status.

3. **Future directions**: Our ongoing study focuses on the biological outcomes triggered by TPS application, including neuronal activation and functional network changes. Future studies have been designed according to the current therapeutic protocol for patients with AD. The longitudinal study involves repeated TPS applications followed by multimodal imaging and behavioral assessment.

the top of the head was depilated and covered with ultrasound gel. The animals from each cohort were equally and randomly assigned to stimulation and sham groups. The sham group of each cohort underwent the respective experimental procedure for the same duration without stimulation, thereby filtering out any effects unrelated to TPS in the relative quantitative comparison. The duration from induction to completion of the TPS application was 30 min.

Cohort I: The animals were continuously monitored with OA imaging for 8 min with a 10-min break halfway. Within this timeframe the animals received two, 4-min TPS applications as described in next sections. Following completion, the animals recovered immediately.

Cohort II: The animals in this cohort received the same TPS treatments as Cohort I without being monitored with OA imaging. Upon completion of the stimulation, the animals received an intraperitoneal (i.p.) bolus injection of 0.08 mL of gadolinium-tetraazacyclododecanetetraacetic acid (Gd-DOTA). The animals were immediately transferred to the 7T MRI scanner (Bruker Biospin, Ettlingen, Germany), positioned on a dedicated mouse bed, and placed within the scanner bore. Image acquisition was conducted with a cryogenically cooled radiofrequency (RF) coil and a T1-weighted two-dimensional (2D) fast low-angle shot (FLASH) sequence, 30 min after the contrast-agent injection, to allow sufficient time for circulation and diffusion.[23] The total duration of the MRI process was 30 min. The animals recovered after the image acquisition.

Following completion of the respective experimental procedure, all animals were transcardially perfused (30 mL phosphate-buffered saline [PBS] followed by 30 mL 4% paraformaldehyde [PFA] in PBS). The brains were extracted, preserved in PFA for 24 h, and then transferred to 30% sucrose for at least 2 days prior to freezing, sectioning, and immunohistochemistry.

2.2 | TPS

TPS was implemented with a clinically-approved TPS handpiece (Neurolith, Storz Medical AG, Switzerland) that delivers ultrashort pulses with duration ≈ 3 μs. The ultrasound beam is focused at 50 mm in the axial direction from the face of the TPS handpiece. It has full width at half maximum (FWHM) of 56 and 5 mm in the axial and lateral directions, respectively. Ultrasound pulses were emitted at a pulse frequency of 4 Hz for a total of 100 pulses with per-pulse energy densities at the focus of 0.05 mJ·mm^{-2} (referred as "low energy") and 0.25 mJ·mm^{-2} (referred as "high energy"), respectively. The low energy level of 0.05 mJ·mm^{-2} is roughly equivalent to the energy of 0.25 mJ·mm^{-2} used in the clinical setting, taking into account the different thicknesses of the skull between humans and mice, whereas the highest allowable energy (0.25 mJ·mm^{-2}) was applied to examine the vessel response and potential adverse effects.

2.3 | Cross-sectional real-time OA tomographic imaging and processing

Real-time OA imaging of the murine cortex during TPS stimulation was performed with a cross-sectional multi-spectral optoacoustic tomography (MSOT) system tailored ad hoc for this purpose. The TPS handpiece was inserted in a rigid custom-made holder to ensure the constant distance from the TPS emitter to the mouse brain. The optical fiber bundle was distributed around the TPS handpiece for uniform illumination. OA signal excitation was tuned to 730, 760, 800, and 850 nm optical wavelengths on a per-pulse basis. The raw data were anonymized prior to post-processing to eliminate any bias. The cross-sectional OA images were reconstructed using a filtered back-projection principle considering signal weighting to minimize the artifacts associated with acoustic scattering and reflections.[24] Prior to reconstruction, the raw data were band-pass filtered. A singular value decomposition (SVD) clutter filter was applied to the reconstructed images, grouped per wavelength, to isolate the signal fluctuations attributed to hemodynamic changes from the static background.[25] For each wavelength, the frames corresponding to the seven different subsets (time intervals) were selected and the maximum intensity projection (MIP) for all frames of each subset was calculated. Frames affected by TPS interferences (<1%) were rejected. Each MIP image was further analyzed to identify vessels with profound changes through the sections. Regions

of interest (ROIs) were generated to isolate such vessels, and the average maximum intensity quantified and compared. The biodistributions of oxygenated (HbO) and deoxygenated (HbR) hemoglobin were estimated by normalizing the single-wavelength images with the optical fluence estimated by imaging the circular face of a cylindrical agar phantom (16 mm diameter) embedding uniformly-distributed black ink positioned at the same location as the mouse scalp, followed by standard spectral fitting of the images at wavelengths different from the absorption spectra of the two forms of hemoglobin.[26] Detailed information on the tomographic imaging and the respective processing can be found in the Supplementary Material.

2.4 | Statistical analysis

All values are expressed as means ± standard deviations (SDs). The statistical analysis was carried out using the absolute intensity values for the effect accuracy. Differences between the means of the groups in the OA analysis were analysed using two-way repeated measures analysis of variance (ANOVA) and in the BBB integrity with one-way ANOVA. The iterative Grubbs' method was used to detect any outliers in all groups and strains.[27] The p values in the OA analysis were adjusted based on the Holm Sidak post hoc correction. Statistical analysis was performed on the mean value obtained per animal. All statistical analyses were performed using Prism 10 (Graphpad).

3 | RESULTS

3.1 | Multiparametric characterization of TPS with multimodal imaging

Multimodal imaging techniques facilitate a deeper understanding of biological processes by combining complementary information from tissue structure and function. It is of particular importance to elucidating complex cerebral dynamics in response to different types of stimuli. Our multimodal imaging platform consisted of preclinical OA and MRI systems to monitor the TPS-induced effects in real time and post-treatment, particularly pertaining hemodynamic changes and potential alterations of BBB integrity. Separate cohorts of mice were imaged with each modality to reduce the induced burden on the animals and to ensure that imaging was performed either during (OA) or immediately after (MRI) TPS exposure (Figure 1A, see Methods for details). TPS stimulation was performed under isoflurane anesthesia with the mice immobilized in a prone position, a standardized body posture allowing for consistency across experiments (Figure 1B). The TPS handpiece emits a relatively wide ultrasound beam simultaneously exciting a large portion of the murine brain (Figure 1B and Figure S1). During the experiments, the TPS beam was directed to the center of the brain to ensure that most brain areas were exposed (Figure 1B). The stimulation paradigm consisted of subsequent application of three sequences, 100 pulses each separated by 1 min with different per-pulse energy densities (Figure 1B, see Methods for details). The same

process was repeated for a second time, 10 min after completion of the first round of stimulations. The low energy level (0.05 mJ·mm^{-2}) is comparable to that used in clinical trials when adjusted for the much thinner skull in mice relative to the human dimensions.[28] The high energy level, corresponding to the maximum intensity emitted by the TPS handpiece (0.25 mJ·mm^{-2}), was used to induce more pronounced responses and to assess potential adverse effects in the brain. A custom setup incorporating the TPS handpiece, a 512-element full-ring ultrasound transducer array, and a multi-arm optical fiber bundle was developed for real-time cross-sectional OA imaging of the murine cortex of Cohort I of mice during TPS stimulation (Figure 1C, see Methods for details). Per-pulse tuning of the laser wavelength enabled capturing multi-spectral (multi-wavelength) images at a sufficiently high frame rate (2 multispectral images per second) to characterize the hemodynamic changes induced by brain activity[29] (Figure 1C). Multi-spectral unmixing enables distinguishing the biodistributions of oxygenated and deoxygenated hemoglobin in the resolved microvascular networks (Figure 1C, see Methods for details), thereby facilitating a comprehensive multi-parametric characterization of the induced changes.[30] Contrast-enhanced MRI (CE-MRI) imaging of Cohort II of mice was performed following TPS stimulation with the same protocol used for Cohort I and additional i.p. administration of gadodiamide (Gd-DTPA, Omniscan, U.S.A.). A cryocoil significantly outperforming standard room temperature coils in terms of sensitivity was employed to image the mouse brain (Figure 1D). Gadolinium diffusion can be captured by image reconstruction as bright diffuse areas in the brain parenchyma, acquired with a T1-weighted fast low-angle shot (or FLASH) sequence.[23] Thereby, a stack of 17 coronal sections was acquired to enable assessing BBB integrity across the entire brain (Figure 1D).

3.2 | Real-time OA monitoring of hemodynamic changes

OA imaging provides the unique capability to simultaneously capture changes in oxygenated (HbO) and deoxygenated (HbR) hemoglobin associated with neurovascular coupling or other hemodynamic responses. The OA imaging system employed was tailored to visualize the entire murine cortex in real time in order to reveal hemodynamic changes during TPS stimulation in CD1, 5xFAD, and 3xTg-AD mouse brains. CD1 mice represent a standard healthy model, whereas 5xFAD and 3xTg-AD mice are established transgenic strains recapitulating AD-related phenotypes for the selected ages (see Methods for details). An increase in OA signal was observed in microvascular networks across a relatively large cortical area following TPS stimulation for all strains. The superposition of the baseline image (maximum intensity from the first 100 frames) and the difference map (baseline image subtracted from the maximum intensity at the last stimulation) offers a full-scale view of the induced effects throughout the entire cortex (Figure 2A). The OA signal intensity at the isosbestic point of hemoglobin (≈800 nm) corresponds to total hemoglobin signal, indicative of blood volume changes associated with vasodilation (Figure S2).
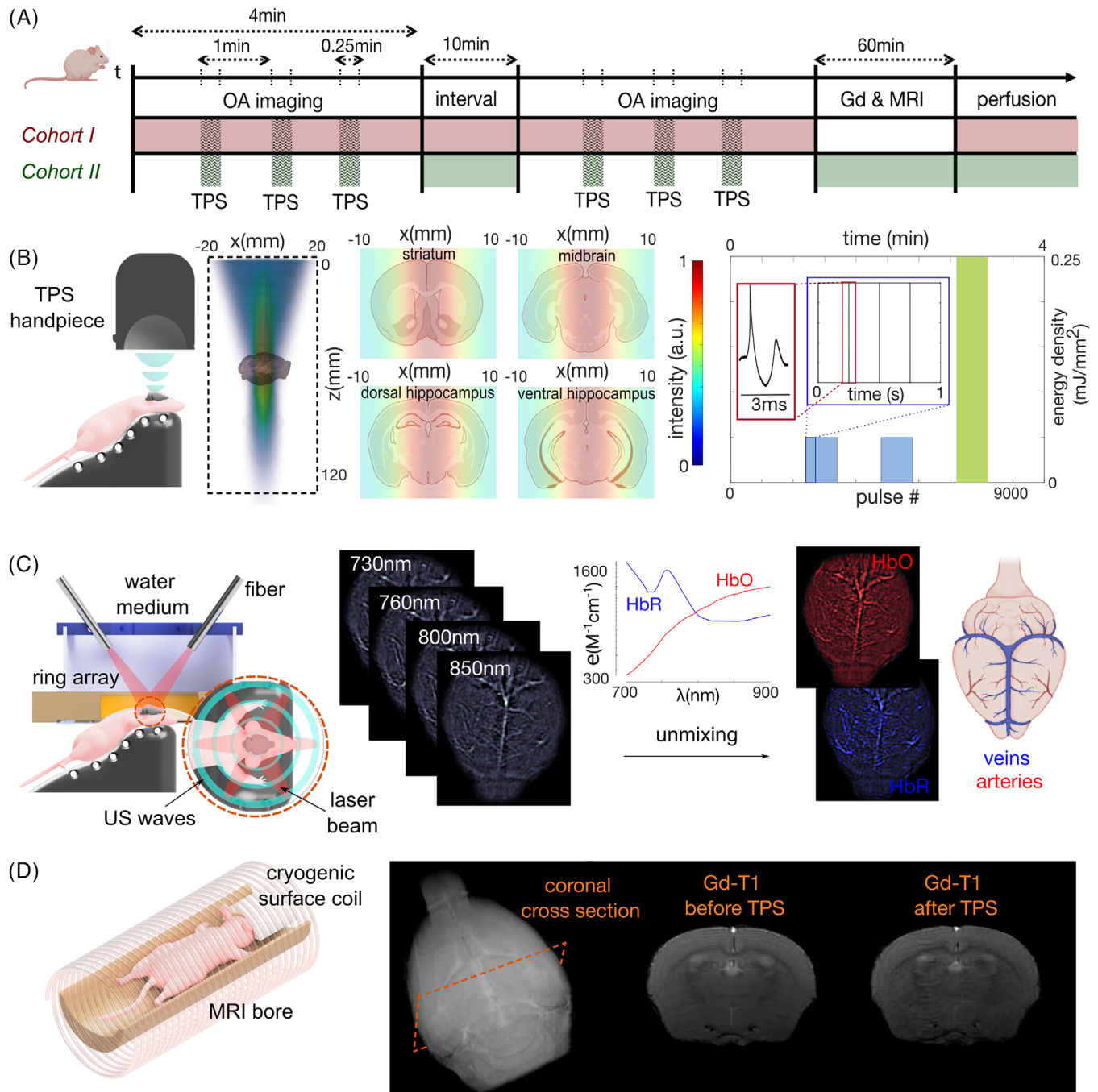
FIGURE 1 Overview of the multimodal imaging study. (A) Timeline of the imaging protocols for two separate cohorts of mice treated with TPS. Cohort I underwent continuous OA imaging while receiving two TPS stimulation sessions separated by a 10-min interval. Cohort II received the same TPS stimulation sessions without OA imaging followed by i.p. injection of Gd-DOTA and MRI 30 min after. (B) TPS configuration for the mice immobilized in a prone position and profile of the emitted ultrasound beam relative to the entire murine brain and brain sections. The ultrasound beam is focused at 50 mm in the axial direction, with FWHM of 56 and 5 mm in the axial and lateral directions, respectively. The stimulation paradigm, consisting of subsequent application of three sequences, 100 pulses each separated by 1 min with different per-pulse energy densities, is shown. Ultra-short pulses with duration 3 µs were emitted at a pulse frequency of 4 Hz for a total of 100 pulses, with per-pulse energy densities at the focus of 0.05 mJ·mm^{-2} and 0.25 mJ·mm^{-2}, respectively. (C) OA imaging configuration. A custom setup incorporating the TPS handpiece, a 512-element full-ring ultrasound transducer array and a multi-arm optical fiber bundle was developed for real-time cross-sectional OA imaging of the murine cortex during TPS stimulation. Per-pulse tuning of the laser wavelength rendered multi-spectral images enabling unmixing of the biodistributions of HbO and HbR based on the spectrally distinctive extinction coefficients (ε) of HbO and HbR. (D) MRI imaging. A cryocoil was employed to image the mouse brain. Gd-DOTA administration can be visualized as bright diffuse areas in the brain parenchyma, acquired with a T1-weighted FLASH sequence. FLASH, fast low-angle shot; FWHM, full width at half maximum; Gd, gadoteric acid; HbO, oxygenated hemoglobin; HbR, deoxygenated hemoglobin; i.p., intraperitoneal; MRI, magnetic resonance imaging; OA, optoacoustic; TPS, transcranial pulse stimulation.
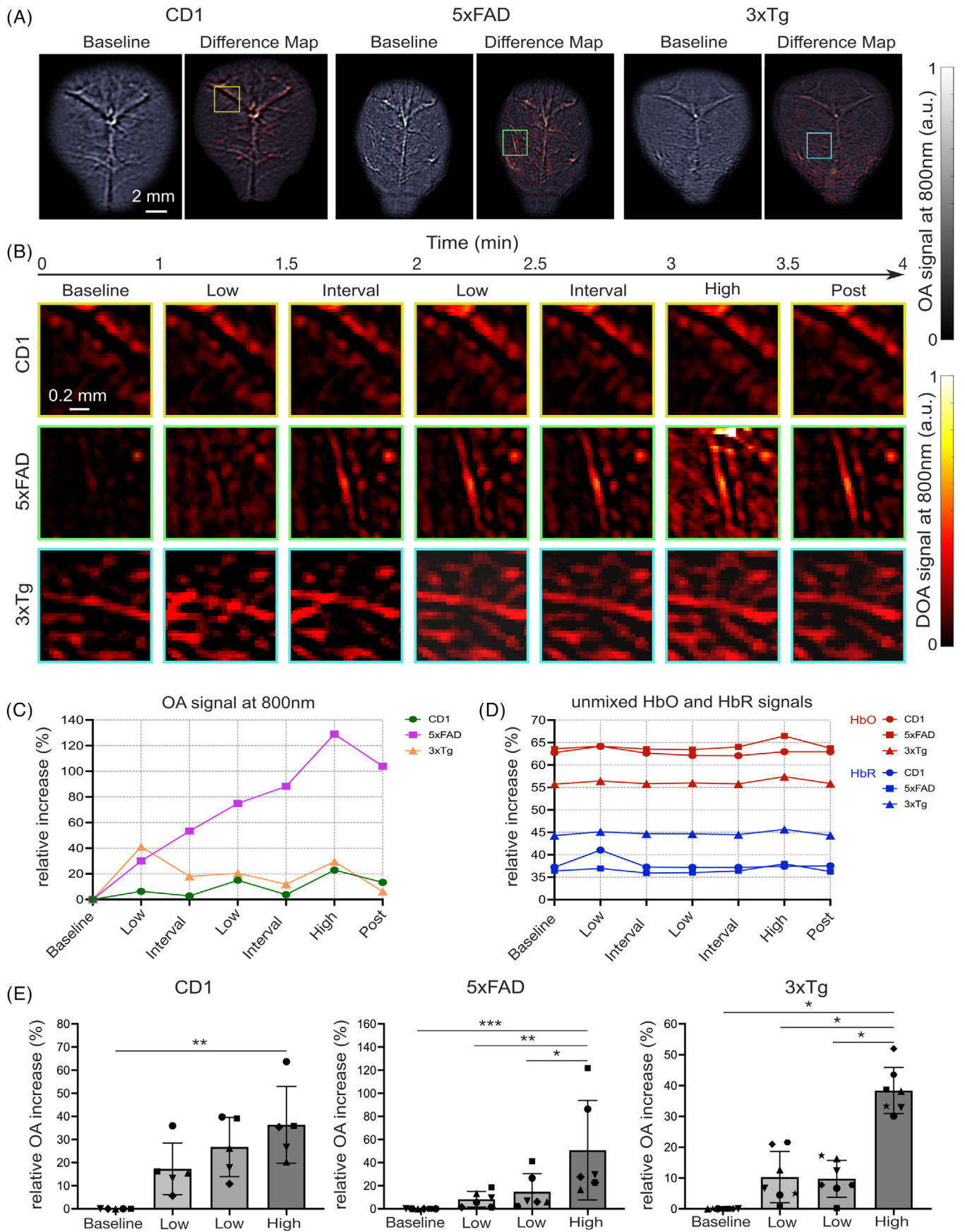
Magnification of selected vessels that exhibited the most prominent changes, as observed in the difference map, enables the visualization of the response dynamics when alternating from stimulation and inactive intervals (Figure 2B). It is important to note that different vessel responses to TPS could be captured within the same brain and across animals (Figure S3). This variability in the cerebrovascular response could be attributed to differences in the vessel diameter and the corresponding mechanics. It has been suggested that arterioles and first-order capillaries dilate first, dictating the increase in cerebral blood flow (CBF) that outweighs the local capillary resistance.[31,32] In the selected CD1 mouse brain example, the vessel-response profile followed the stimulation pattern. An intensity increase of 6%, 15%, and 23% compared to the baseline was observed at the respective stimulation intervals, whereas the intensity dropped during the inactive intervals (Figure 2C). In the selected 5xFAD mouse brain example, the vessel intensity increased over the course of the stimulation and inactive intervals, reaching a maximum of 129% when TPS was applied at the highest energy setting (Figure 2C). In the selected 3xTg-AD mouse brain example, the vessel responded to the first stimulation by an observed intensity increase on the order of 40% compared to the baseline intensity, followed by an intensity drop at the inactive interval (Figure 2C). The vessel intensity increased only when the TPS handpiece was emitting pulses, yet at lower values compared to the first stimulation (Figure 2B,C). The patterns for the selected vessels in all mice confirmed the heterogeneities in the observed responses (Figure S3), with some vessels responding to all three TPS stimulation intervals and others to only one or two of them. In some cases the OA intensity at the selected vessel kept increasing after a given stimulation sequence. In others, a switch behavior was observed, where the vessel intensity increased only during the stimulation sequence and then returned to baseline. In most cases, the strongest response was observed for the high-energy TPS sequence, with a few exceptions probably due to saturation effects (Figure 2B,C, Figure S3).

Heterogeneous dynamic patterns were observed in the unmixed biodistributions of oxygenated and deoxygenated hemoglobin for the selected vessels. Changes in the oxygenation level normalized to the baseline total hemoglobin signal are shown in Figure 2D for the representative vessels from each mouse strain. Generally, changes in HbO and HbR are linked to a complex combination of nitric oxide–induced vasodilation as well as neurovascular coupling and metabolic changes associated with brain activity.[33,34]

The responses to the stimulation events revealed statistically significant differences to the baseline intensity (Figure 2E). For the CD1 mouse brains, the OA signal intensity at the last TPS session was significantly higher compared to the baseline (40.4%, $p = 0.0043$). The average vessel intensity in the 5xFAD mouse brains was found significantly higher during the last stimulation compared to the baseline and all other stimulation intervals (percent change: baseline-third stimulation: 49.7%, $p = 0.0007$; first-third stimulation: 38.0%, $p < 0.0035$; second-third stimulation 28.9%, $p < 0.0161$). In accordance with the 5xFAD strain, the OA signal intensity of the 3xTg-AD mouse brain was found to be significantly higher at the last stimulation compared to the baseline and the other two stimulation sessions at lower energy levels (percent change: baseline-third stimulation: 39.9%, $p = 0.0273$; first-third stimulation: 27.7%, $p = 0.0306$; second-third stimulation 27.9%, $p = 0.0306$).

The analysis and comparison of the sham to the stimulated brains is presented in the Supplementary Material. As expected, qualitative evaluation of the sham CD1 and 5xFAD brain vasculature did not show any prominent vessel changes throughout the 10-min OA imaging interval (Figure S4). Quantitative analysis confirmed the absence of significant vessel responses, whereas OA intensity changes were retained within a ± 10% range from the baseline, that served as the error range in our analysis (Figures S3 and S5). The comparison between the stimulation intervals is presented as percent change to capture the relative change; however, the statistical analysis was carried out using the absolute intensity values for the effect accuracy.

3.3 | BBB integrity following TPS

It is essential to confirm that TPS stimulation is driving the observed hemodynamic changes and not a potential BBB opening induced by the treatment. Although microbubbles were not injected in this study, it is still possible that excess energy transfer to the brain could result in a BBB compromise. Therefore, the brains of TPS-treated and sham CD1, 5xFAD, and 3xTg-AD mice were examined in vivo and ex vivo in terms of brain integrity with methods providing different (increasing)

FIGURE 2 Hemodynamic responses in CD1, 5xFAD, and 3xTg mice visualized with OA imaging. (A) Baseline OA images (maximum intensity from the first 100 frames) and difference maps (baseline OA images subtracted from the maximum intensity of the OA images during the last stimulation) for the isosbestic point of hemoglobin (≈800 nm). (B) Difference maps for ROIs indicated in (A) corresponding to selected vessels with conspicuous changes across time. (C) Percent changes of the OA signal intensity at 800 nm in the selected ROIs revealing variability in the hemodynamic responses to TPS. (D) Changes in the unmixed biodistributions of HbO and HbR for the selected vessels normalized to the baseline total hemoglobin (HbT = HbO+HbR). (E) Statistical analysis of the OA signal changes at 800 nm for all CD1, 5xFAD, and 3xTg mice used in the study. The values displayed are normalized to the baseline for better visualization, but statistical analysis was performed using the unnormalized data. For CD1 mice, a significant difference in OA signal intensity at the last TPS session relative to the baseline was observed (40.4% increase, $p = 0.0043$). For 5xFAD mice, significant differences in OA signal intensity for the last stimulation compared to the baseline and other stimulation intervals were observed (percent change: baseline-third stimulation: 49.7%, $p = 0.0007$; first-third stimulation: 38.0%, $p < 0.0035$; second-third stimulation 28.9%, $p < 0.0161$). For 3xTg mice, significant differences in the OA signal intensity at the last stimulation compared to the baseline and the other two stimulation intervals at lower energy levels were observed (percent change: baseline-third stimulation: 39.9%, $p = 0.0273$; first-third stimulation: 27.7%, $p = 0.0306$; second-third stimulation 27.9%, $p = 0.0306$). HbO, oxygenated hemoglobin; HbR, deoxygenated hemoglobin; OA, optoacoustic; ROIs, regions of interest; TPS, transcranial pulse stimulation.

(A) CD1 sham | CD1 stim | 5xFAD stim | 3xTg stim | 3xTg sham (PC)

(B) Glut-1 NeuN
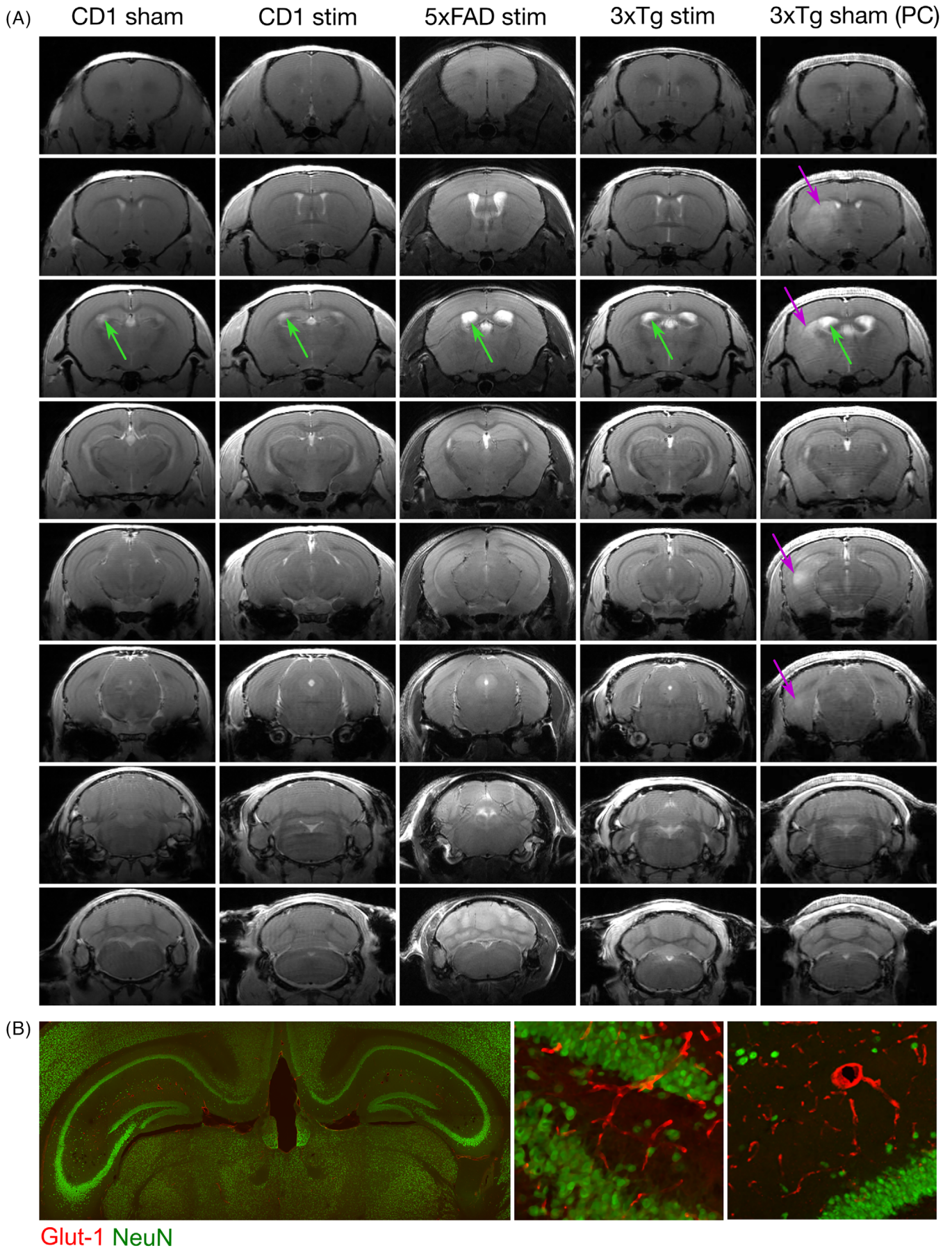
sensitivity levels (Figure 3 and Figure S6). Evans blue dye was used initially to examine leakage in the brain indicative of BBB opening, since the dye does not cross the BBB when intact. Gross pathology of representative TPS-treated and sham CD1 mice did not show any BBB disruption (Figure S6), which is clearly visible in mice with a compromised BBB.[35] MRI is the preferred imaging method for brain applications given its non-ionizing and non-invasive nature. MRI coupled with i.p. injection of gadolinium reveals sites of BBB permeability, since this contrast agent cannot cross the intact BBB. CE-MRI coronal slices of CD1, 5xFAD, and 3xTg-AD mouse brains showed no contrast agent leakage in the parenchyma, an indicator of an impermeable BBB (Figure 3A). The presence of contrast is, however, recognized by the bright signal in the vasculature as well as in one of the 3xTg-AD sham brains, arguably corresponding to the disease phenotype (Figure 3A, violet arrow). The brain with the spontaneously permeable BBB was used for quantitative analysis as a positive control of the method. The average intensity of both hemispheres was computed for all 17 brain slices and compared against a healthy sham brain and the mouse brain with permeable BBB. As expected, the treated brains do not differ from the untreated sham brain but have statistically lower intensity values compared to the impacted BBB ($p < 0.0001$; CD1: 56%, 5xFAD: 53%, 3xTgAD: 52%) (Figure S7B). The MR images provide another interesting insight: the enlargement of the lateral ventricles (LVs) of both AD strains compared to the CD1 brain examples (Figure 3A, green arrow). Quantification of the LVs revealed a 3.5-fold volume increase ($p < 0.0001$) in the AD brains compared to the CD1 brains at the age of the experiment (Figure S7A). This phenomenon has been reported to occur in these AD mouse strains.[36,37] Although not intended for quantitative analysis, immunohistochemistry was also performed to visualize the BBB integrity. Glut-1 (red) is a hydrophobic protein that aids in the transport of glucose across the BBB and is expressed in endothelial cells, astrocytes, and choroid plexus, which make up the BBB. NeuN (green) is a neuronal differentiation marker and was included in the staining to visualize neuronal density. Imaging at lower and higher magnification settings revealed a healthy populated hippocampal structure with a complex vessel network that could be observed through the cross-sections (Figure 3B). A closer look into the CA subregion shows the vessel branching around the neurons (Figure 3B).

4 | DISCUSSION

The primary purpose of this study was to assess alterations in cerebral hemodynamics and BBB permeability in mice by using a multi-modal methodology. Real-time monitoring of brain hemodynamics and oxygenation was achieved with a state-of-the-art OA tomographic system customized to facilitate transverse cross-sectional imaging of the murine brain during repeated TPS exposure. Specifically, gadolinium-enhanced MRI confirmed that the brain architecture was maintained intact without BBB opening after TPS exposure, establishing the safety profile of the procedure. Moreover, increased OA signal was detected systematically during stimulation, suggesting increased CBF. This was followed by a subsequent return to baseline levels for some mice, whereas it was sustained after stimulation for others. Saturation effects during repeated stimulations were also observed. The statistically significant differences among the stimulation intervals and the baseline evinced response differences between healthy and diseased mice. The CD1 brains responded to every stimulation interval, whereas significant responses were observed only for the high-energy stimulation interval in AD brain vessels. This observation suggests that higher energy, yet within the safety window, is necessary to induce hemodynamic changes in the AD mice, probably due to their pathological vessels. Indeed, we observed cerebral amyloid angiopathy associated with accumulation of amyloid on the vessel walls in 3xTg mice (Figure S8). Capillary constriction driven by contractile pericytes, evoked, probably, by oligomeric amyloid beta ($A\beta$), is a primary biomarker for AD.[38,39] Moreover, CBF reduction has been implicated in driving the cognitive decline in patients with AD. Given the role of CBF in the initial stages of AD, TPS stimulation could reverse the pathological vasoconstriction and halt cognitive deterioration, offering an essential breakthrough in AD treatment. In addition, the pathological capillary constriction in AD patients compared to healthy controls justifies the necessity of higher intensity to increase the blood flow in the transgenic animal models. This observation highlights an important aspect in the treatment planning, that brain integrity at the time of treatment should drive the development of personalized protocols. Apart from the pathological vessels, the LV enlargement was evident for AD mice relative to CD1 healthy controls in the CE-MRI coronal images. Similarly, the rate of ventricular volume increase has been a proposed biomarker for AD progression, as it correlates with an increase in senile plaques and neurofibrillary tangles.[40] Little is known of the ventricular response to ultrasound, yet a recent study indicated enhanced cortical cerebrospinal fluid (CSF) influx during FUS stimulation in rodents.[41] These findings are promising, but whether TPS under the examined protocol triggered a CSF response should be explored. The observations regarding the ventricular pathology, however, indicate pathological progression of the disease and could be correlated with hindered blood flow.

FIGURE 3 Screening of BBB integrity with MRI. (A). CE-MRI coronal slices acquired following i.p. injection of Gd-DOTA are shown for a sham (untreated) CD1 brain, TPS-treated CD1, 5xFAD, and 3xTg brains, and a PC sham 3xTg brain featuring spontaneous BBB impairment (magenta arrows). The images confirm the absence of Gd-DOTA in the brain parenchyma, an indicator of impermeable BBBs. The presence of contrast is apparent by the bright signal in the vasculature, evincing the enlargement of the LVs of both AD strains relative to CD1 mice (green arrows). (B) Immunohistochemical analysis of a stimulated CD1 mouse brain to visualize the BBB integrity with the anti-Glut-1 (red) and anti-NeuN (green). Imaging at lower and higher magnification settings revealed a healthy populated hippocampal structure with a complex vessel network that could be observed through the cross-sections. AD, Alzheimer's disease; BBB, blood–brain barrier; CE, contrast-enhanced; Gd-DOTA, gadoteric acid; i.p., intraperitoneal; LVs, lateral ventricles; MRI, magnetic resonance imaging; PC, positive control; TPS, transcranial pulse stimulation.

The vascular responses reported herein are consistent with those of previous studies tracking cerebral hemodynamic alterations in response to ultrasound treatments.[42,43] Low-energy extracorporeal shock wave application has also been shown previously to promote the release of nitric oxide in other organs, consequently resulting in an increase in blood flow.[44–46] Nitric oxide is growingly recognized to have a therapeutic role in many conditions, for example, due to cytoprotective effects stemming from its capacity to enhance local blood flow and neutralize highly reactive free radicals.[47] Moreover, ultrasound has been shown to activate mechanosensitive ion channels through increases in membrane tension,[48] and neuronal responses detected by the increase in calcium signals in cerebral cortical structures during and following ultrasound neuromodulation.[49]

5 | CONCLUSION

In conclusion, this study highlights the potential of TPS as a non-invasive therapy for AD, demonstrating its safety and measurable effects in the murine brain. We capitalized on the unique in vivo imaging capabilities of our multi-modal preclinical imaging platform to provide valuable insights into the hemodynamic effects of TPS, notably observing the increase in blood volume within microvascular networks without compromising the BBB integrity. Moreover, we provide evidence of the dynamic relationship between AD pathology, blood flow constriction, and the necessary TPS intensity for therapeutic effects. These results pave the way for further exploration and optimization of TPS, facilitating advancements in therapeutic strategies for AD.

CONFLICT OF INTEREST STATEMENT

The authors declare no conflicts of interest. Author disclosures are available in the Supporting information.

CONSENT STATEMENT

The current study was conducted with animal models in accordance with the Swiss Federal Act on Animal Protection and approved by the Cantonal Veterinary Office Zürich.

ORCID

Maria Eleni Karakatsani https://orcid.org/0000-0002-8368-1360

REFERENCES

1. 2022 Alzheimer's disease facts and figures. *Alzheimers Dement.* 2022;18:700-789.
2. GBD 2019 Dementia Forecasting Collaborators. Estimation of the global prevalence of dementia in 2019 and forecasted prevalence in 2050: an analysis for the Global Burden of Disease Study 2019. *Lancet Public Health.* 2022;7:e105-e125.
3. X Li, X Feng, X Sun, N Hou, F Han, Y Liu. Global, regional, and national burden of Alzheimer's disease and other dementias, 1990-2019. *Front Aging Neurosci.* 2022;14:937486.
4. C Ballard, D Aarsland, J Cummings, et al. Drug repositioning and repurposing for Alzheimer disease. *Nat Rev Neurol.* 2020;16:661-673.
5. DS Knopman, H Amieva, RC Petersen, et al. Alzheimer disease. *Nat Rev Dis Primers.* 2021;7:33.
6. X Li, M Ji, H Zhang, et al. Non-drug therapies for Alzheimer's disease: A review. *Neurol Ther.* 2023;12:39-72.
7. Meng Y, Hynynen K, Lipsman N. Applications of focused ultrasound in the brain: from thermoablation to drug delivery. *Nat Rev Neurol.* 2021;17:7-22.
8. Nicodemus NE, Becerra S, Kuhn TP, et al. Focused transcranial ultrasound for treatment of neurodegenerative dementia. *Alzheimers Dement.* 2019;5:374-381.
9. C Gasca-Salas, B Fernández-Rodríguez, JA Pineda-Pardo, et al. Blood-brain barrier opening with focused ultrasound in Parkinson's disease dementia. *Nat Commun.* 2021;12:779.
10. SH Park, K Baik, S Jeon, WS Chang, BS Ye, JW Chang. Extensive frontal focused ultrasound mediated blood–brain barrier opening for the treatment of Alzheimer's disease: A proof-of-concept study. *Transl Neurodegener.* 2021;10:44.
11. T Welton, F Cardoso, JA Carr, et al. Essential tremor. *Nat Rev Dis Primers.* 2021;7:83.
12. Blackmore DG, Razansky D, Götz J. Ultrasound as a versatile tool for short-and long-term improvement and monitoring of brain function. *Neuron.* 2023;111:1174-1190.
13. Kamimura HA, Conti A, Toschi N, Konofagou EE. Ultrasound neuromodulation: Mechanisms and the potential of multimodal stimulation for neuronal function assessment. *Front Phys.* 2020;8:150.
14. C Rabut, S Yoo, RC Hurt, et al. Ultrasound technologies for imaging and modulating neural activity. *Neuron.* 2020;108:93-110.
15. ME Karakatsani, R Ji, MF Murillo, et al. Focused ultrasound mitigates pathology and improves spatial memory in Alzheimer's mice and patients. *Theranostics.* 2023;13:4102.
16. Truong DQ, Thomas C, Hampstead BM, Datta A. Comparison of transcranial focused ultrasound and transcranial pulse stimulation for neuromodulation: a computational study. *Neuromodulation.* 2022;25:606-613.
17. R Beisteiner, E Matt, C Fan, et al. Transcranial pulse stimulation with ultrasound in Alzheimer's disease—a new navigated focal brain therapy. *Adv Sci.* 2020;7:1902583.
18. Chen X, You J, Ma H, Zhou M, Huang C. Transcranial pulse stimulation in Alzheimer's disease. *CNS Neurosci Ther.* 2024;30:e14372.
19. Popescu T, Pernet C, Beisteiner R. Transcranial ultrasound pulse stimulation reduces cortical atrophy in Alzheimer's patients: a follow-up study. *Alzheimers Dement.* 2021;7:e12121.
20. Beisteiner R, Hallett M, Lozano AM. Ultrasound neuromodulation as a new brain therapy. *Adv Sci.* 2023;10:2205634.
21. GT Shinzato, T Assone, PC Sandler, et al. Non-invasive sound wave brain stimulation with transcranial pulse stimulation (TPS) improves neuropsychiatric symptoms in Alzheimer's disease. *Brain Stimulation.* 2024;17:413-415.
22. H Lohse-Busch. Long-term results of Alzheimers' dementia treated with transcranial pulse stimulation. *Alzheimers Dement.* 2023;19:e082078.
23. ME Karakatsani, T Kugelman, R Ji, et al. Unilateral focused ultrasound-induced blood-brain barrier opening reduces phosphorylated tau from the rTg4510 mouse model. *Theranostics.* 2019;9:5396.
24. Deán-Ben XL, Ntziachristos V, Razansky D. Artefact reduction in optoacoustic tomographic imaging by estimating the distribution of acoustic scatterers. *J Biomed Opt.* 2012;17:110504-110504.

25. C Demene, T Deffieux, M Pernot, et al. Spatiotemporal clutter filtering of ultrafast ultrasound data highly increases Doppler and fUltrasound sensitivity. *IEEE Trans Med Imaging*. 2015;34:2271-2285.

26. Tabulated Molar Extinction Coefficient for Hemoglobin in Water. 1998. omlc.org/spectra/hemoglobin/summary.html

27. Aslam M. Introducing Grubbs's test for detecting outliers under neutrosophic statistics–An application to medical data. *J King Saud Univ Sci*. 2020;32:2696-2700.

28. Estrada H, Rebling J, Turner J, Razansky D. Broadband acoustic properties of a murine skull. *Phys Med Biol*. 2016;61:1932.

29. J Robin, R Rau, B Lafci, et al. Hemodynamic response to sensory stimulation in mice: comparison between functional ultrasound and optoacoustic imaging. *Neuroimage*. 2021;237:118111.

30. Z Chen, I Gezginer, M-A Augath, et al. Simultaneous functional magnetic resonance and optoacoustic imaging of brain-wide sensory responses in mice. *Adv Sci*. 2023;10:2205191.

31. N Renaudin, C Demené, A Dizeux, N Ialy-Radio, S Pezet, M Tanter. Functional ultrasound localization microscopy reveals brain-wide neurovascular activity on a microscopic scale. *Nat Methods*. 2022;19:1004-1012.

32. JR Mester, MW Rozak, A Dorr, M Goubran, JG Sled, B Stefanovic. Network response of brain microvasculature to neuronal stimulation. *Neuroimage*. 2024;287:120512.

33. Zhu WM, Neuhaus A, Beard DJ, Sutherland BA, DeLuca GC. Neurovascular coupling mechanisms in health and neurovascular uncoupling in Alzheimer's disease. *Brain*. 2022;145:2276-2292.

34. Drew PJ. Neurovascular coupling: motive unknown. *Trends Neurosci*. 2022;45:809-819.

35. Yi Kung, C-H Wu, M-T Lin, W-H Liao, W-S Chen, M-Y Hsiao. Blood-cerebrospinal fluid barrier opening by modified single pulse transcranial focused shockwave. *Drug Deliv*. 2023;30:97-107.

36. Santos CY, Snyder PJ, Wu WC, Zhang M, Echeverria A, Alber J. Pathophysiologic relationship between Alzheimer's disease, cerebrovascular disease, and cardiovascular risk: a review and synthesis. *Alzheimers Dement*. 2017;7:69-87.

37. DD Quintana, Y Anantula, JA Garcia, et al. Microvascular degeneration occurs before plaque onset and progresses with age in 3xTg AD mice. *Neurobiol Aging*. 2021;105:115-128.

38. Korte N, Nortley R, Attwell D. Cerebral blood flow decrease as an early pathological mechanism in Alzheimer's disease. *Acta Neuropathol*. 2020;140:793-810.

39. Goldsmith HS. Alzheimer's disease: a decreased cerebral blood flow to critical intraneuronal elements is the cause. *J Alzheimers Dis*. 2022;85:1419-1422.

40. SM Nestor, R Rupsingh, M Borrie, et al. Ventricular enlargement as a possible measure of Alzheimer's disease progression validated using the Alzheimer's disease neuroimaging initiative database. *Brain*. 2008;131:2443-2454.

41. S Choi, J Kum, SY Hyun, et al. Transcranial focused ultrasound stimulation enhances cerebrospinal fluid movement: Real-time in vivo two-photon and widefield imaging evidence. *Brain Stimul*. 2024;17:1119-1130.

42. Yuan Y, Wang Z, Liu M, Shoham S. Cortical hemodynamic responses induced by low-intensity transcranial ultrasound stimulation of mouse cortex. *Neuroimage*. 2020;211:116597.

43. Aurup C, Bendig J, Blackman SG, et al. Transcranial Functional ultrasound imaging detects focused ultrasound neuromodulation induced hemodynamic changes in mouse and nonhuman primate brains in vivo. *Biorxiv*. 2024; https://doi.org/10.1101/2024.03.08.583971

44. B Liu, Y Zhang, Na Jia, et al. Study of the safety of extracorporeal cardiac shock wave therapy: observation of the ultrastructures in myocardial cells by transmission electron microscopy. *J Cardiovasc Pharmacol Ther*. 2018;23:79-88.

45. D Hayashi, K Kawakami, K Ito, et al. Low-energy extracorporeal shock wave therapy enhances skin wound healing in diabetic mice: a critical role of endothelial nitric oxide synthase. *Wound Repair Regen*. 2012;20:887-895.

46. O Goertz, J Hauser, T Hirsch, et al. Short-term effects of extracorporeal shock waves on microcirculation. *J Surg Res*. 2015;194:304-311.

47. Kumar S, Singh RK, Bhardwaj T. Therapeutic role of nitric oxide as emerging molecule. *Biomed Pharmacother*. 2017;85:182-201.

48. Sorum B, Rietmeijer RA, Gopakumar K, Adesnik H, Brohawn SG. Ultrasound activates mechanosensitive TRAAK K+ channels through the lipid membrane. *Proc Natl Acad Sci*. 2021;118:e2006980118.

49. Xu R-S, Wu X-M, Xiong Z-Q. Low-intensity ultrasound directly modulates neural activity of the cerebellar cortex. *Brain Stimul*. 2023;16:918-926.

SUPPORTING INFORMATION

Additional supporting information can be found online in the Supporting Information section at the end of this article.